Unified Equivalent Circuit Model and Optimal Design of V^2 Controlled Buck Converters

Shuilin Tian, *Student Member, IEEE*, Fred C. Lee, *Life Fellow, IEEE*, Qiang Li, *Member, IEEE*, and Yingyi Yan, *Member, IEEE*

***Abstract*—V^2 control has advantages of simple implementation and fast transient response and is widely used in industry for point-of-load applications. This control scheme is elegant when output capacitors with large *RC* time constant are employed, such as OSCON capacitors. However, in most cases using capacitors with small *RC* time constant, such as ceramic capacitors, instability problem will occur. Previous modeling methods including sampled-data modeling, discrete-time analysis, time-domain analysis, and describing function are all very mathematical and difficult to apply for practical engineers as little physical insight can be extracted. Up to now, no equivalent circuit model is proposed which is able to predict the instability issue and serve as a useful design tool for V^2 control. This paper proposes a unified equivalent circuit model which is applicable to all types of capacitors by considering the effect of capacitor voltage ripple. The equivalent circuit provides the physical insight of V^2 control as a nonideal voltage source, a dual concept of previous nonideal current source for current-mode control. The equivalent circuit model is a simple yet accurate complete model and is very helpful for design purpose. Optimal design guidelines for point-of-load applications are provided. The proposed equivalent circuit model is applicable to both variable frequency modulation and constant frequency modulation. The equivalent circuit model and design guidelines are verified with Simplis simulation and experimental results.**

***Index Terms*—Equivalent circuit model,, optimal design guidelines, ripple-based control, V^2 control.**

I. Introduction

V^2 control architecture, and its variety named ripple-based control, as shown in Fig. 1, has been widely applied in point-of-load buck converters [1]–[11]. Compared with the traditional voltage-mode control and current-mode control, this control structure has the following three features: 1) No current sensing network is required. 2) Fast load transient characteristics with direct output voltage feedback. 3) The outer-loop compensator is much simpler; usually a simple integrator with low bandwidth is adequate. The outer-loop compensation is shown as the green dash line in Fig. 1 since the integrator can be further eliminated in many applications, which is called ripple-based control in the literature [12], [13].

V^2 control concept can be implemented as constant frequency modulation (including constant frequency V^2 peak control [14]–[23] or constant frequency V^2 valley control [24], [35]) or variable frequency modulation (including constant on-time V^2 control [25]–[32], [55] and constant off-time V^2 control [1], [2]). Among the four, constant on-time V^2 control [3]–[8], [52]–[53] and constant frequency V^2 peak control [9]–[11] are most popular in commercial products. In industry products, various names are used based on their own understanding on constant on-time V^2 control structure: for example, Texas Instruments D-CAP, D-CAP+, and D-CAP2 control products [3], [52]; Maxim's Quick-PWM control products [6], [53] and National Semiconductor's constant on-time control products [7].

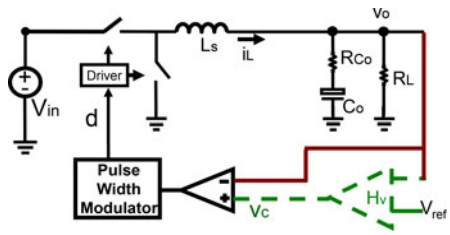

Fig. 1. Structure of V^2 control (with outer-loop compensator shown in dash line) and ripple-based control (without outer-loop compensator).

This control scheme works well using output capacitor with large *RC* time constant, such as OSCON capacitors. However, when small *RC* time constant capacitors, such as ceramic capacitors, are used, subharmonic oscillations occur in most cases. For quantitative analysis and system design purpose, an accurate model is necessary. The modeling of this circuit is very challenging as the nonlinear pulse width modulator (PWM) becomes very complicated because not only the inductor current information is fed back to the modulator but also the capacitor voltage ripple information. The early models proposed in [15]–[17], and [33]–[34] directly extends Dr. Ridley's sample and hold the concept [60] of peak current-mode control to constant frequency V^2 peak control, without any justification. Generally speaking, extension of sample and hold concept is not applicable for V^2 implementation since this concept is from constant frequency current-mode control, which just considers the sideband information of the current loop and does not consider the influence of the capacitor voltage ripple. This is why the models used in [15]–[17], and [33], [34] cannot accurately predict the influence from the capacitor voltage ripple in constant frequency V^2 peak control.

To accurately predict the influence from the capacitor voltage ripple in V^2 control, several methods are proposed. In [12], Krylov–Bogoliubov–Mitropolsky algorithm is used to reconstruct the switching ripple from state-space averaged models and, therefore, to improve the accuracy of the model. However,

Manuscript received June 1, 2014; revised February 24, 2015; accepted April 14, 2015. Date of publication April 21, 2015; date of current version September 29, 2015. Recommended for publication by Associate Editor C. Fernandez.

The authors are with the Center for Power Electronics Systems, the Bradley Department of Electrical and Computer Engineering, Virginia Tech, Blacksburg, VA 24061 USA (e-mail: tianshuilinpe@gmail.com; fclee@vt.edu; lqvt@vt.edu; yanyingyi@gmail.com).

Color versions of one or more of the figures in this paper are available online at http://ieeexplore.ieee.org.

Digital Object Identifier 10.1109/TPEL.2015.2424913

it is too complex for practical use. In [13] and [38]–[41], the sampled-data modeling techniques are employed to derive the stability criterion by judging whether the eigenvalues are less than unity in discrete-time domain. For sampled-data modeling method, it is conducted in discrete-time domain and is difficult for practical engineers. In [35]–[37], the general discrete-time analysis is applied on constant frequency V^2 valley control and constant on-time V^2 control. In [42], accurate analysis based on discrete-time modeling and Floquet theory is presented. However, these discrete-time analyses are based on the numerical analysis and no symbolic expression can be extracted and very little physical insight is provided. In [43]–[45], the time-domain analysis is used based on the calculation of the inductor current information, the compensation ramp, and the charge variation of the output capacitor. The model based on this method can accurately predict the stability criterion of V^2 control and the magnitude of the ramp compensations to avoid instability. However, only the critical stability point can be predicted and no design guideline can be provided with a certain stability margin.

For most of power electronics engineers, continuous-domain small-signal analysis is preferred. The most successful continuous-domain model of V^2 control is derived based on the describing function (DF) method by Dr. Li and Lee [46], [49], [56]. The control-to-output and output impedance transfer functions of V^2 control are derived and summarized in [46]. The instability issue when using ceramic capacitors can be well predicted. However, the model is incomplete as audio susceptibility and input impedance are still lacking. Furthermore, as all the feedback information is lumped together with complicated mathematical derivation, little physical insight is provided. Besides, the mathematical derivation of this model is very complicated and time consuming. The tedious rederivation process limits its application to the modified version of V^2 control. As an example, for Texas Instruments D-CAP2 control products, a current sensing network with a high-pass filter is added into the original V^2 control. Up to now, there is no small-signal model published for this control structure based on the DF method.

Equivalent circuit model, on the other hand, can eliminate previous disadvantages and has already been a powerful tool for the analysis of dc–dc converters with traditional voltage-mode control [57] and current-mode control [58], [59]. For equivalent circuit model of V^2 control, however, no satisfactory result has been proposed. A design-oriented equivalent circuit model for V^2 control is proposed in [47]. A significant issue of this equivalent circuit model is that it failed to explain the output impedance characteristic of V^2 control. In [48], an equivalent circuit model based on current-mode control is proposed for V^2 control. For capacitors with large *RC* time constant, such as Tantalum capacitor and OSCON capacitor, this model is accurate. However, the derivation of the model makes an assumption that the voltage ripple across the pure capacitance is negligible comparing with the voltage ripple across the ESR. Therefore, the model is not applicable to capacitors with small *RC* time constant, such as ceramic capacitors. Deriving an equivalent circuit model which is applicable to V^2 control with different kinds of capacitors is a remaining challenging task for researchers.

In this paper, a unified equivalent circuit model for V^2 control is proposed. The equivalent circuit model has clear physical meaning and is very helpful for design. One example is provided to demonstrate the value of the equivalent circuit model by showing how simple it is to predict the transfer functions of enhanced constant on-time V^2 control with high-pass filter. As a comparison, it is very complicated to redo the DF to derive the transfer function. This paper is an extension of the original conference paper [50] and has more emphasis on design aspects. The remaining of this paper is organized as follows: Section II analyzes the sideband effect in V^2 control and derives the equivalent circuit model for constant on-time V^2 control. Section III discusses the physical meaning of the model. Section IV discusses design guideline for constant on-time V^2 control with ceramic capacitors in point-of-load applications. Section V extends the equivalent circuit model to other V^2 control schemes and small-signal performances are compared between V^2 controls with different modulation schemes. Simulation and experimental results are presented in Section VI. Finally, a summary is given in Section VII.

II. Equivalent Circuit Model Development of Constant On-Time V^2 Control

A. Sideband Effect Analysis in V^2 Control

In switching-mode power converter, the PWM is nonlinear. When control signal has small-signal perturbation with frequency f_m, the modulator generates multiple frequency components: fundamental component (f_m), the switching frequency component ($f_{\rm sw}$) and its harmonics ($n^* f_{\rm sw}$), and the sideband components ($f_{\rm sw} \pm f_m, nf_{\rm sw} \pm f_m$).

For traditional voltage-mode control, state-space average concept has been well established [63]. With averaging concept, switching frequency component is eliminated and, therefore, the sideband component is not considered. In [62], the reason why the average model loses accuracy when modulation frequency is close to half of switching frequency is explained by the sideband effect: with closed loop, additional f_m is generated when the sideband frequency $f_{\rm sw} - f_m$ goes through modulator. This part of f_m is ignored in average model which makes the average concept loses its accuracy in high-frequency range. In the example shown in [62], for a 1-MHz switching converter, in the 400-kHz bandwidth design, the average model is good only up to 100 kHz, i.e., one-tenth of the switching frequency. Taking into consideration of the sideband effect, a multifrequency small-signal model is proposed for buck converters with voltage-mode control in [62] and the model is applicable beyond half of the switching frequency.

For current-mode control, the scenario is similar but more complex as the sideband of inductor current needs to be considered in inner current loop [61]. It is very hard to consider the sideband effects directly in the frequency-domain, and time-domain analysis is utilized in the DF modeling approach in [59] and [61]. The DF method is applied to the closed-loop time-domain waveform to model the nonlinear current-mode modulator. By doing so, the sideband effect of the inductor current has been taken into consideration and the model is accurate even beyond switching frequency. An equivalent circuit model, which has clear physical insight, is proposed based on the nonideal current source concept in [58], [59], and [61]. The nonidealness of the current

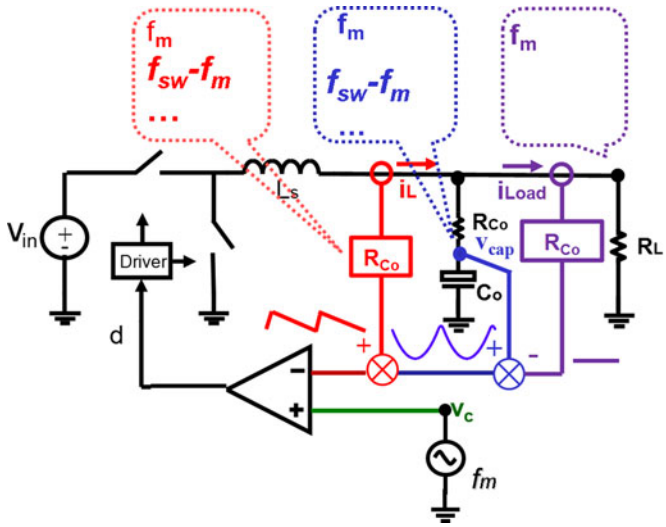

Fig. 2. Frequency spectrum of direct feedback loop of V^2 control with three feedback paths.

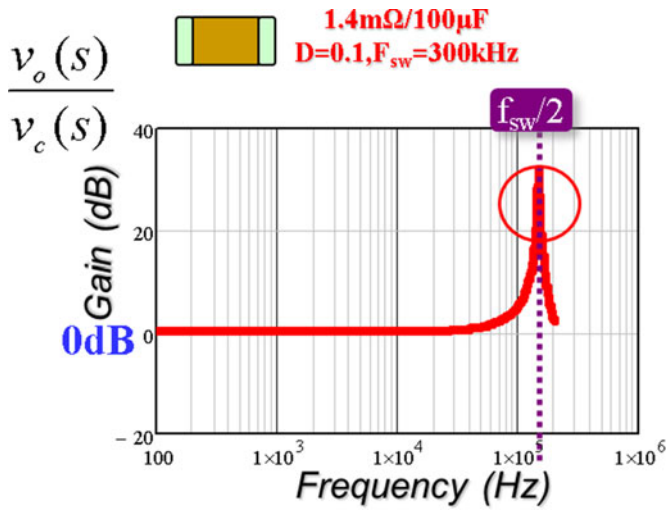

Fig. 3. Bode plot of control-to-output voltage transfer function for ceramic capacitor (1.4 mΩ/100 μF).

source is caused by the sideband effect of inductor current: for peak current-mode control, it causes a pair of double poles at half of switching frequency. For constant on-time current-mode control, it causes a pair of double poles at $1/(2^*D^*f_{\rm sw})$: When D is small, the double pole is at very high frequency and its effect is small. Therefore, for constant on-time current mode with small duty cycle, inductor current sideband effect can be neglected and the current source can be regarded as ideal.

For V^2 control, the scenario is even more complicated than current-mode control. The output voltage is the sum of the voltage across ESR and the voltage across the capacitance. The voltage across ESR contains information of the inductor current and load current. Therefore, from modeling point of view, the direct feedback of output voltage can be separated into three parts

$$v_{\rm o} = i_{Co} \cdot R_{Co} + v_{\rm cap} = i_L \cdot R_{Co} - i_{\rm Load} \cdot R_{Co} + v_{\rm cap}. \tag{1}$$

Fig. 2 explicitly shows three feedback paths and shows the frequency spectrum of each feedback path when control signal is under modulation. Similar as current-mode control, inductor current feedback does not have a low-pass filter, so all the sidebands ($f_{\rm sw} - f_m$, $f_{\rm sw} + f_m$, etc.) are fed back to the modulator and the sideband effect needs to be considered. The capacitor voltage loop is a direct feedback without any compensation. Therefore, the sidebands of capacitor voltage also need to be taken into consideration. As a result, the scenario in V^2 control is even more complicated than current-mode control: not only does the inductor current sideband effect needs to be considered, but also the capacitor voltage sideband effect.

The fact that both the sidebands of inductor current and capacitor voltage participate in modulation makes it extremely difficult for modeling in frequency domain. Similar as in current-mode control, the most successful continuous small-signal model is derived in [46] based on the DF method. Both sidebands of inductor current and capacitor voltage are included and the model is accurate up to switching frequency. The control-to-output transfer function of constant on-time V^2 control for small D is shown in the following [46]:

$$\frac{v_{\rm o}(s)}{v_c(s)} \approx \frac{(R_{Co}C_{\rm o}s+1)}{\left(1+\frac{s}{Q_3\omega_2}+\frac{s^2}{\omega_2^2}\right)}$$

$$Q_3 = \frac{T_{\rm sw}}{\pi\left(R_{Co}C_{\rm o}-\frac{T_{\rm on}}{2}\right)}, \qquad \omega_2 = \frac{\pi}{T_{\rm sw}}. \tag{2}$$

As shown in Fig. 3, the gain is unity (0 dB) up to frequency close to $1/2f_{\rm sw}$, where a pair of double poles occurs. This indicates that physically capacitor voltage loop turns the converter into a nonideal voltage source. The quality factor of the double pole is related with capacitor parameters. This pair of double poles is caused by capacitor voltage sideband, as inductor current sideband effect can be neglected for constant on-time modulation with small duty cycle [61].

B. Equivalent Circuit Development of Constant On-Time V^2 Control

As shown in the previous analysis, the buck converter with V^2 control can be regarded as a nonideal voltage source. To derive an equivalent circuit model to represent this nonideal voltage source, the methodology is to establish the connection between V^2 control and current-mode control, as the equivalent circuit model of current-mode control is well established in [58], [59] and [61]. The circuit shown in Fig. 2 is manipulated by combining the control signal, load current, and capacitor voltage, as shown in Fig. 4(a). The combination signal v_{c2} is used as a reference to control the inductor current. Note that v_{c2} contains the information as follows:

$$v_{c2}(f_m) = v_{c1}(f_m) - v_{\rm cap}(f_m) - v_{\rm cap}(f_{\rm sw} - f_m). \tag{3}$$

With this manipulation, equivalent circuit model of current-mode control in [61] can be employed, as shown in Fig. 4(b). Compared with current-mode control, two more current sources

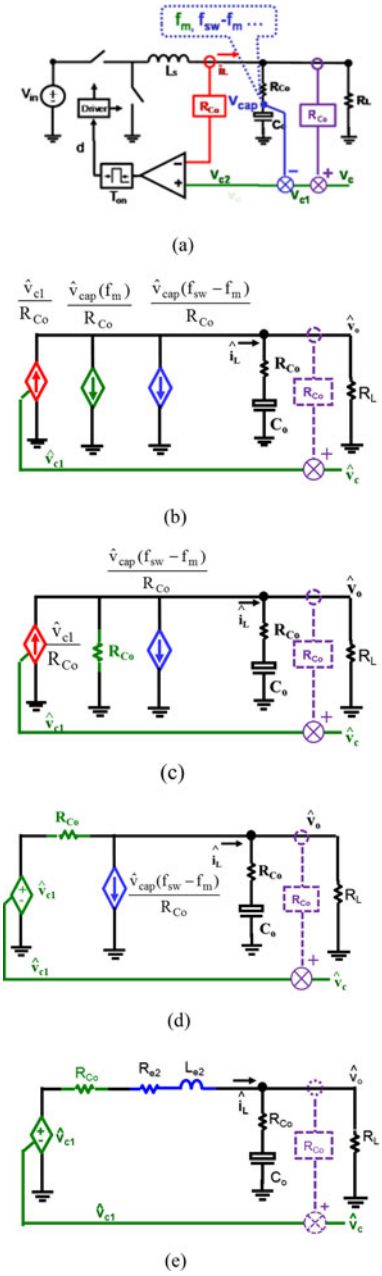

Fig. 4. Derivation of equivalent circuit model of constant on-time V^2 control for small *D*. (a) Combine control signal, load current, and capacitor voltage as reference for inductor current. (b) Employ equivalent circuit model for current-mode control in [61]. (c) Use resistor to represent current source controlled by modulation frequency of capacitor voltage. (d) Transforming to a voltage source using Thevenin's theorem. (e) Use $R_{e2} - L_{e2}$ branch to represent current source controlled by sideband of capacitor voltage.

appeared in V^2 control. To understand the contribution of the green current source which is controlled by the modulation frequency of capacitor voltage, the following assumption is made:

$$\hat{v}_{\rm cap}(f_m) \approx \hat{v}_{\rm o}(f_m). \tag{4}$$

The magnitude of the green current source is $\hat{v}_{\rm o}/R_{Co}$, while the voltage across the current source is $\hat{v}_{\rm o}$. Therefore, this current source essentially is a resistor with the magnitude of R_{Co},

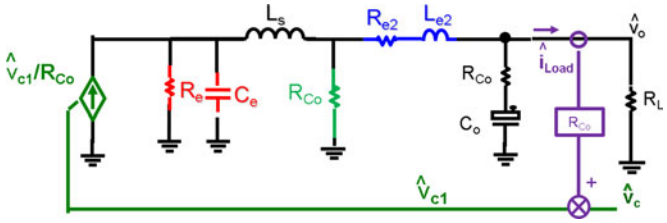

Fig. 5. Equivalent circuit model of constant on-time V^2 considering double poles caused by inductor current sidebands.

as shown in Fig. 4(c). With Thevenin's theorem, it is clear that modulation frequency of capacitor voltage feedback actually turns the current source into a voltage source, as shown in Fig. 4(d).

In current-mode control, the inductor current sideband effect is represented by an impedance comprised by R_e and C_e, which will resonate with power stage inductor to form a pair of double poles at high frequency [61]. For V^2 control, capacitor voltage sideband also causes a pair of double poles, as shown in Fig. 3. Using similar concept, it is assumed that the effect of capacitor voltage sideband is equivalent to an impedance comprised by R_{e2} and L_{e2}, as shown in Fig. 4(e). This impedance resonates with output capacitor to represent the double pole at $\frac{1}{2}f_{\rm sw}$. Based on the result shown in (2), the expression of R_{e2} and L_{e2} can be derived as follows:

$$R_{e2} = -R_{Co} - \frac{T_{\rm on}}{2C_{\rm o}}, \qquad L_{e2} = \frac{{T_{\rm sw}}^2}{\pi^2 C_{\rm o}}. \tag{5}$$

The transfer function shown in (2) is an approximated transfer function which is only valid under small *D* case. When *D* is becoming larger, the effect of an additional pair of double poles caused by inductor current sideband needs to be considered as it will cause additional phase delay at high frequency [46]. The control-to-output voltage transfer function which is applicable for the whole duty cycle range is shown as follows [46]:

$$\frac{v_{\rm o}(s)}{v_c(s)} \approx \frac{(R_{Co}C_{\rm o}s+1)}{\left(1+\frac{s}{Q_1\omega_1}+\frac{s^2}{\omega_1^2}\right)\left(1+\frac{s}{Q_3\omega_2}+\frac{s^2}{\omega_2^2}\right)}, Q_1 = \frac{2}{\pi},$$
$$\omega_1 = \frac{\pi}{T_{\rm on}}, Q_3 = \frac{T_{\rm sw}}{\pi(R_{Co}C_{\rm o} - T_{\rm on}/2)}, \quad \omega_2 = \frac{\pi}{T_{\rm sw}}. \tag{6}$$

The scenario turns out to be very interesting as one pair of double poles is caused by capacitor voltage sideband and another pair of double poles is caused by inductor current sideband. From the knowledge of the current-mode control [61], the double poles caused by inductor current sideband indicates that the inductor is a nonideal current source. The expression of this double pole is same as constant on-time current-mode control shown in [61]. Therefore, we can directly employ the equivalent circuit model for constant on-time current-mode control to represent this double pole, as shown in Fig. 5, where the expression of R_e and C_e is shown as follows:

$$R_e = 2L_s/T_{\rm on}, \qquad C_e = T_{\rm on}^2/(L_s\pi^2). \tag{7}$$

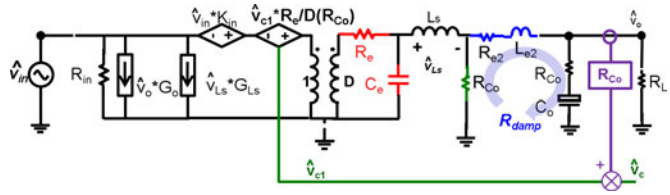

Fig. 6. Complete equivalent circuit model of constant on-time V^2 control.

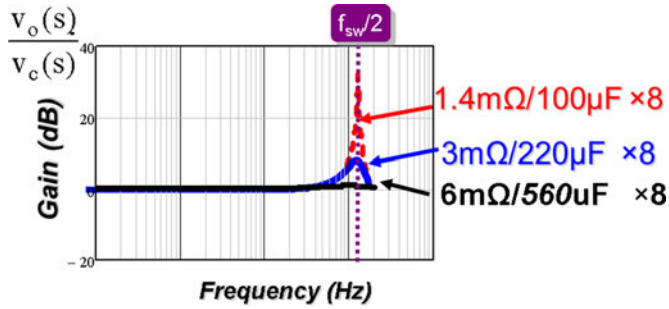

Fig. 7. Comparisons of control-to-output voltage transfer function with different output capacitors.

Using the same derivation strategy as the three-terminal switch model for current-mode control in [58], the input property can also be considered and the complete model for constant on-time V^2 control is shown as Fig. 6, where the expressions of $R_{\rm in}, G_{Ls}, G_{\rm o}, K_{\rm in}$ are shown as follows:

$$R_{\rm in} = -\frac{V_{\rm in}}{DI_c}, \qquad G_{Ls} = \frac{I_c}{V_{\rm in}},$$
$$G_{\rm o} = \left(\frac{I_c}{V_{\rm in}} - \frac{D}{R_{Co}}\right), \qquad K_{\rm in} = \frac{D'}{D}. \tag{8}$$

III. Discussion of the Equivalent Circuit Model

A. Physical Meaning of Equivalent Circuit

The equivalent circuit model reveals that the inductor current feedback turns the power stage into a nonideal current source. The nonidealness of this current source is shown in equivalent circuit by resonance between virtual C_e and power stage inductor L_s, which forms a pair of double poles at $1/(2D)^* f_{\rm sw}$. The capacitor voltage feedback turns current source into a nonideal voltage source. The nonidealness of this voltage source is shown in equivalent circuit by resonance between virtual L_{e2} and output capacitor C_o, which forms another pair of double poles at $\frac{1}{2}f_{\rm sw}$. The strategy to represent double poles caused by inductor current sideband and capacitor voltage sideband is very similar: inductor current sideband effect is represented by resonance between a virtual capacitor C_e and power stage inductor L_s, while capacitor voltage sideband effect is represented by resonance between a virtual inductor L_{e2} and power stage capacitor C_o. For constant on-time V^2 control, the capacitor voltage sideband may make the circuit unstable. The damping factor of the double poles caused by capacitor voltage sideband is determined by the damping resistance $R_{\rm damp}$ in the resonance loop. The expressions of the damping resistor $R_{\rm damp}$ and the quality factor of the double poles are shown as follows:

$$R_{\rm damp} = R_{Co} - \frac{T_{\rm on}}{2C_{\rm o}}$$
$$Q_3 = \frac{1}{R_{\rm damp}}\sqrt{\frac{L_{e2}}{C_{\rm o}}} = \frac{T_{\rm sw}}{\pi\left(R_{Co}C_{\rm o} - \frac{T_{\rm on}}{2}\right)}. \tag{9}$$

$R_{\rm damp}$ can be negative or positive depending on capacitor parameter, which means that the double poles may lie in right-half plane and the circuit may run into instability problem.

B. Capacitor Parameter Effect on Dynamic Performance

Using OSCON capacitors (6 mΩ/560 μF), $R_{\rm damp}$ is 710 μΩ, which is large and Q_3 is around 0.3, R_{e2} and L_{e2} in Fig. 4(e) in this case can be neglected, and it is a well-controlled voltage source. For a comparison, for a special ceramic capacitor (3 mΩ/220 μF), $R_{\rm damp}$ is 280 μΩ and Q_3 is 2.5; although it is stable, there is a large peaking shown in Fig. 7, which means that the dynamic performance is bad. For another type of traditional ceramic capacitor (1.4 mΩ/100 μF), $R_{\rm damp}$ is −33 μΩ, the circuit is unstable.

The methods to solve the instability problem and optimal design of the parameters will be discussed in Section IV.

IV. Design Guideline for Constant On-Time V^2 Control Using Ceramic Capacitors

A. Using Controlled ESR Ceramic Capacitor for Portable Electronics Applications

As shown in Fig. 7, there is a right-half-plane double pole when traditional ceramic capacitors are used, which indicates that the circuit is unstable. In time domain, subharmonic oscillation occurs. On the other hand, ceramic capacitors are preferred in portable electronics applications due to the small size. To solve the instability problem, one simple solution is to employ controlled ESR ceramic capacitors [54]: TDK Corporation recently provides options to customize ESR for ceramic capacitors. With this technology, the ESR of the ceramic capacitors can be customized without increasing the ESL value. For V^2 application, (9) can be used for customization of ESR so that the double pole at $\frac{1}{2}f_{\rm sw}$ is well damped: for example, ESR can be customized such that $Q_3 = 1$. As shown in Fig. 8, with traditional ceramic capacitors (10 uF/3 mΩ), the peaking at $\frac{1}{2}f_{\rm sw}$ is large. With the ESR customized to 200 mΩ, the peaking is eliminated as Q_3 is around 1. With the customized ESR products, conceptually the ripple voltage across ESR overwhelms the ripple voltage across pure capacitance, which is similar as OSCON capacitor case. The disadvantage of this controlled ESR approach is that as the output voltage ripple is increased due to increased ESR, more capacitors need to be paralleled to meet the output voltage ripple requirement. Besides, only a few products are available with limited capacitance value, such as 1 μF and 10 μF. For large capacitance value such as 100 μF, up to now, no customized ESR ceramic capacitors are available. This limitation prevents controlled ESR capacitors as a solution in applications where large capacitance is required.

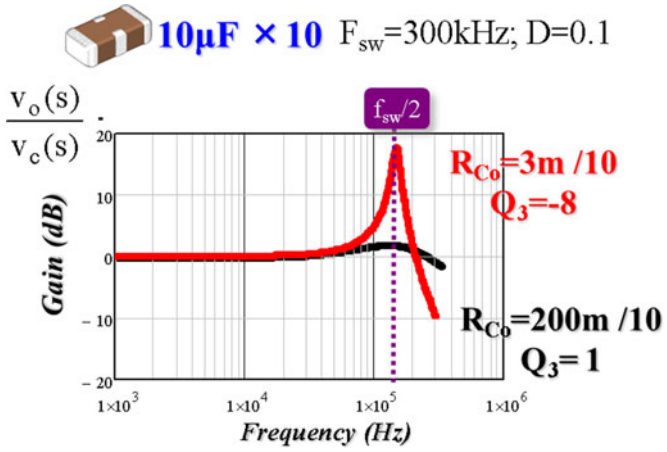

Fig. 8. Customization of ESR for ceramic capacitors to improve dynamic performance.

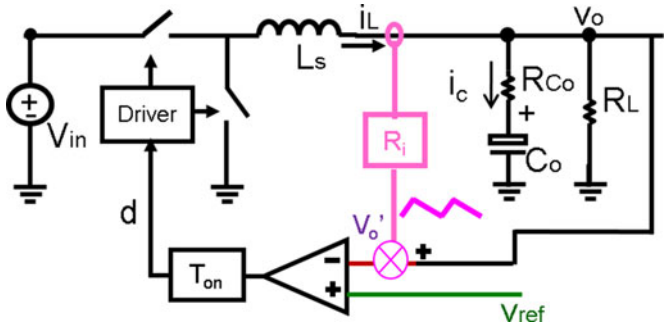

Fig. 9. Diagram of enhanced constant on-time V^2 control.

B. Enhanced V^2 Control with High-Pass Filter for Point-of-Load Application

The second method is to enhance current feedback by adding inductor current ramp, as shown in Fig. 9. Traditional inductor current sensing methods can be used and this method is widely used in industry products [3], [4]. This structure is called enhanced constant on-time V^2 control.

Following the same strategy, the equivalent circuit model can be easily extended to enhanced constant on-time V^2 control, as shown in Fig. 10. The control-to-output voltage for enhanced constant on-time V^2 control is shown as follows:

$$\frac{v_o(s)}{v_c(s)} \approx \frac{(R_{Co}C_o s+1)}{\left(1+\frac{s}{Q_3'\omega_2}+\frac{s^2}{\omega_2^2}\right)}$$

$$Q_3' = \frac{T_{sw}}{\pi\left((R_{Co}+R_i)C_o - T_{on}/2\right)}, \quad \omega_2 = \frac{\pi}{T_{sw}}. \tag{10}$$

The principle for the design of R_i is similar as the controlled ESR ceramic capacitor case: design R_i to control the quality factor of double pole at $½f_{sw}$. As an example, for the traditional ceramic capacitor ($8 \times 100\ \mu\text{F}/1.4\ \text{m}\Omega$), a flat gain can be achieved by adding $R_i = 1.4\ \text{m}\,\Omega$.

However, by adding inductor current information, adaptive voltage positioning is observed in time domain due to the dc

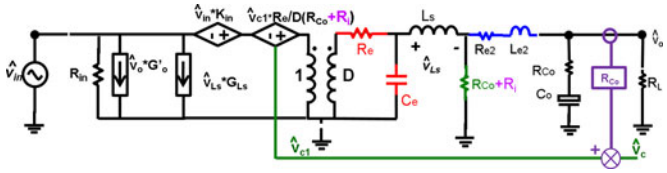

Fig. 10. Complete equivalent circuit model for enhanced constant on-time V^2 control.

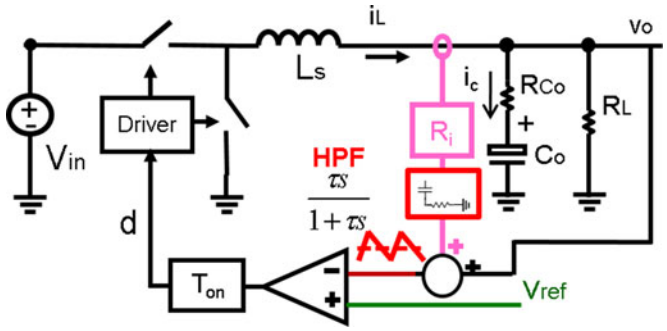

Fig. 11. Addition of high-pass filter to eliminate dc current information.

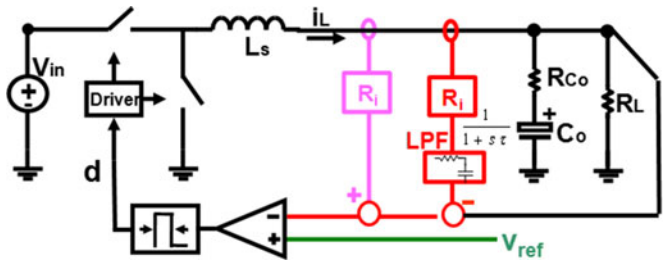

Fig. 12. Modeling strategy: Separating high-pass filter into two paths.

information of inductor current. In many point-of-load applications, output voltage should be well regulated and adaptive voltage positioning is undesired. To eliminate the steady-state droop voltage, a high-pass filter is inserted after current sensing in commercial products [3], [4], as shown in Fig. 11.

Up to now, there is no small-signal model provided for enhanced constant on-time V^2 control with high-pass filter case. The proposed equivalent circuit model can be easily extended to this case with similar modeling strategy: the sensed current information after high-pass filter is manipulated as the subtraction of two signals: one is direct current feedback and the other is the sensed current information flowing through a low-pass filter, as shown in Fig. 12.

As the purpose of high-pass filter is to eliminate the dc information of inductor current while keeping its switching frequency information, the pole position of the filter is designed to be much lower than switching frequency as follows:

$$\tau >> \frac{T_{sw}}{2\pi}. \tag{11}$$

As a result, all the switching frequency component and sidebands is in direct feedback path (pink in Fig. 12), while the low-pass-filter path (red in Fig. 12) only has modulation fre-

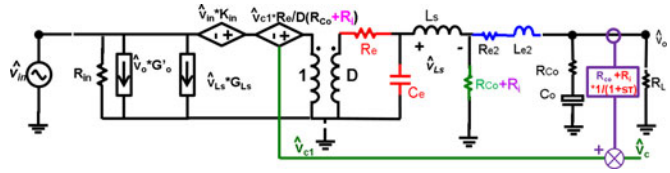

Fig. 13. Complete equivalent circuit model for enhanced constant on-time V^2 control with high-pass filter.

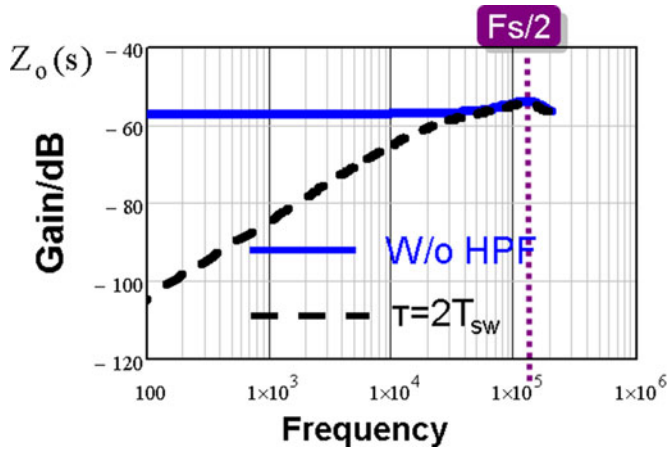

Fig. 14. Improvement of output impedance due to high-pass filter.

quency component. Therefore, equivalent circuit model with high-pass filter can be derived, as shown in Fig. 13.

The output impedance can be obtained as follows:

$$Z_o(s) \approx R_i \left(\frac{\tau s}{1+\tau s}\right) \frac{(R_{Co}C_o s+1)}{\left(1+\frac{s}{Q_3'\omega_2}+\frac{s^2}{\omega_2^2}\right)}. \quad (12)$$

As shown in Fig. 14, the high-pass filter reduces the low-frequency output impedance as expected. The simulation result will be provided in Section VI to prove the accuracy of the equivalent circuit model.

C. V^2 Control with Capacitor Current for Point-of-Load Application

The third method reported in the literature is to enhance current feedback by adding capacitor current [21], [29], [64] as shown in Fig. 15. To sense capacitor current, a simple lossless capacitor current sensing method has been proposed in [29]. Alternatively, a noninvasive capacitor current sensing method which considers the ESL effect has been proposed in [21].

Following the similar strategy, the equivalent circuit model with capacitor current can be derived as shown in Fig. 16.

The only difference between inductor current ramp and capacitor current ramp is the different load current feedback gain: for inductor current ramp case, it is R_{Co}, while for capacitor current ramp case, it is the sum of R_{Co} and R_i. The control-to-output transfer functions of the two cases are almost the same, as the role of load current feedback is negligible in both cases. Therefore, the design of R_i is the same as the inductor current

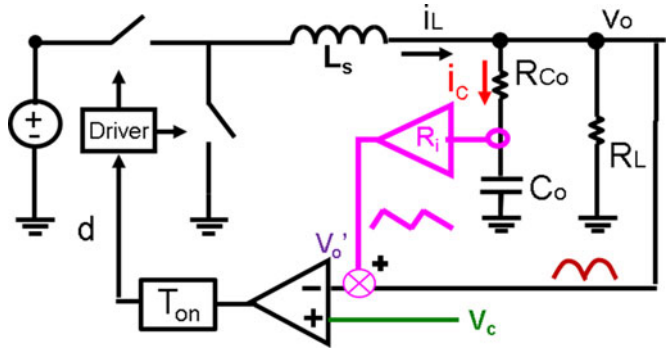

Fig. 15. Diagram of constant on-time V^2 control with capacitor current ramp.

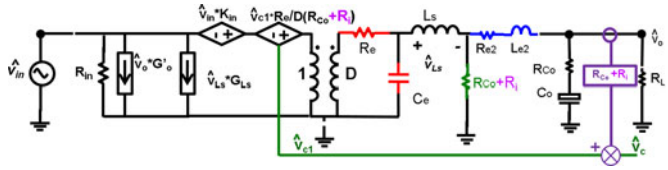

Fig. 16. Complete equivalent circuit model for constant on-time V^2 control with capacitor current.

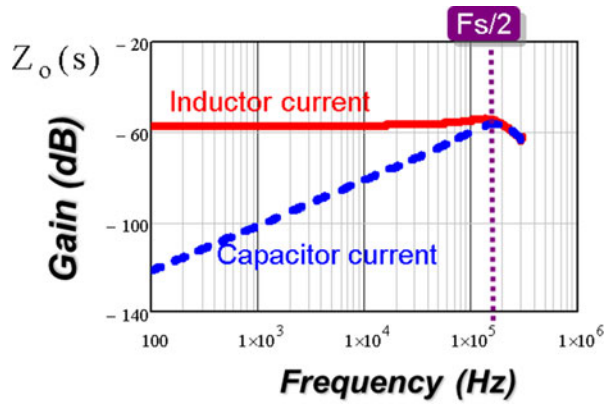

Fig. 17. Output impedance comparisons between inductor current and capacitor current.

ramp case: design R_i to control the quality factor of double pole at $\frac{1}{2}f_{sw}$ is shown in (10).

The output impedance with capacitor current ramp can be derived as follows:

$$Z_o \approx \frac{T_{on}}{2}(R_{Co}+R_i)\cdot s\frac{1+R_{Co}C_o s}{1+\frac{s}{Q_3\omega_2}+\frac{s^2}{\omega_2^2}}. \quad (13)$$

As shown in Fig. 17, while the output impedance is determined by R_i for inductor current ramp, by adding capacitor current ramp, the output impedance is still very low, which means it can still achieve very fast transient response. For practical application, the influence on accuracy of sensed current due to the parasitic parameters (such as ESL effect of the capacitor, ESL due to trace) needs to be taken into consideration. This is one reason why it is not as popular as inductor current in commercial products.

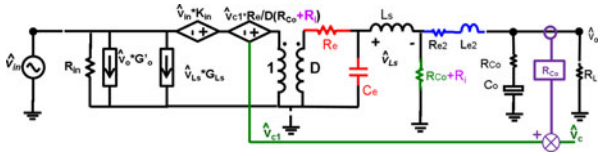

Fig. 18. Unified equivalent circuit model of V^2 control for different modulation schemes.

V. Extension to Other V^2 Control Schemes

Fig. 18 shows a unified equivalent circuit model for V^2 control, the model includes inductor current ramp R_i for all modulation schemes as it is needed to improve the dynamic performance when traditional ceramic capacitors are employed. Besides, the model also includes external ramp compensation in constant frequency V^2 control, as it is required to solve the instability problem in large duty cycle applications [51].

The difference between different V^2 control structures is that the damping and position of the double poles caused by the inductor current loop and capacitor voltage loop are different. As a result, expressions of R_e, C_e, L_{e2}, and R_{e2} are different. The expressions for constant on-time, constant off-time, constant frequency V^2 peak, and constant frequency V^2 valley are shown in (14)–(17), respectively. Note that the equivalent circuit model for constant frequency V^2 control is only valid for relatively small external ramp, i.e., $S_e \le S_f$ for peak V^2 control, which is good enough for design purpose [51]

$$\begin{aligned} R_e &= 2L_s/T_{\rm on}, \qquad C_e = T_{\rm on}^2/(L_s\pi^2) \\ R_{e2} &= -R_{Co} - \frac{T_{\rm on}}{2C_{\rm o}}, \qquad L_{e2} = \frac{T_{\rm sw}^2}{\pi^2 C_{\rm o}} \end{aligned} \tag{14}$$

$$\begin{aligned} R_e &= 2L_s/T_{\rm off}, \qquad C_e = T_{\rm off}^2/(L_s\pi^2) \\ R_{e2} &= -R_{Co} - \frac{T_{\rm off}}{2C_{\rm o}}, \qquad L_{e2} = \frac{T_{\rm sw}^2}{\pi^2 C_{\rm o}} \end{aligned} \tag{15}$$

$$\begin{aligned} R_e &= \frac{L_s}{T_{\rm sw}(0.5 - D + D\cdot s_e/s_f)} \\ C_e &= T_{\rm sw}^2/(L_s\pi^2) \\ R_{e2} &= -R_{Co} - \frac{T_{\rm off}}{2C_{\rm o}}, \qquad L_{e2} = \frac{T_{\rm sw}^2}{\pi^2 C_{\rm o}} \end{aligned} \tag{16}$$

$$\begin{aligned} R_e &= \frac{L_s}{T_{\rm sw}(0.5 - D' + D'\cdot s_e/s_f)} \\ C_e &= T_{\rm sw}^2/(L_s\pi^2) \\ R_{e2} &= -R_{Co} - \frac{T_{\rm sw}}{2C_{\rm o}}, \qquad L_{e2} = \frac{T_{\rm sw}^2}{\pi^2 C_{\rm o}}. \end{aligned} \tag{17}$$

Using constant frequency V^2 peak control as an example, the double pole caused by the inductor current loop is located at $\frac{1}{2}f_{\rm sw}$ and the current loop may also be unstable, depending on the circuit parameter such as duty cycle and the external ramp magnitude. Besides, although the double pole position caused by the capacitor voltage loop is at $\frac{1}{2}f_{\rm sw}$ for all modulation schemes, the damping of the double pole is also different. For constant frequency V^2 peak control, the damping resistance and the quality factor of the double pole is shown as the following:

$$\begin{aligned} R_{\rm damp} &= R_{Co} - \frac{T_{\rm sw}}{2C_{\rm o}} \\ Q_3 &= \frac{1}{R_{\rm damp}}\sqrt{\frac{L_{e2}}{C_o}} = \frac{T_{\rm sw}}{\pi(R_{Co}C_{\rm o} - \frac{T_{\rm sw}}{2})}. \end{aligned} \tag{18}$$

Comparing with (9), with the same circuit parameters, the quality factor of the double pole at $\frac{1}{2}f_{\rm sw}$ for constant frequency V^2 peak control is always larger than constant on-time V^2 control. Therefore, from the stability point of view, constant on-time V^2 control has better performance.

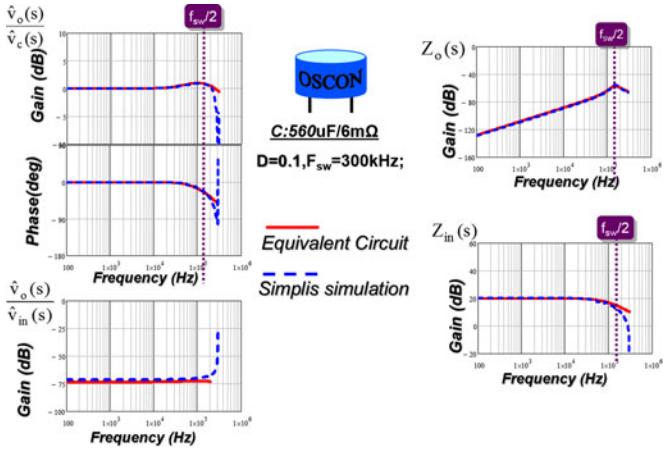

Fig. 19. Simplis verification for constant on-time V^2 control with OSCON capacitors (6 mΩ/560 μF).

VI. Simulation and Experimental Results

Fig. 19 shows the simulation verification for OSCON capacitors (6 mΩ/560 μF), $D = 0.1$ and $f_{\rm sw} = 300$ kHz. All four transfer functions, i.e., control-to-output, audio susceptibility, output impedance, and input impedance are compared. The proposed model agrees with simulation results very well up to 2/3 of $f_{\rm sw}$ for all transfer functions.

Fig. 20 shows the verification for constant on-time V^2 control with ceramic capacitors (3 mΩ/220 μF); $D = 0.1$ and $f_{\rm sw} = 300$ kHz. The proposed equivalent circuit model can predict the peaking of double pole at $\frac{1}{2}f_{\rm sw}$ very well; the output impedance, input impedance, and audio susceptibility also agree very well with simulation results.

Fig. 21 shows the simulation verification for enhanced constant on-time V^2 control with the following parameters: Eight ceramic capacitors (1.4 mΩ/100 μF), $D = 0.1$, $f_{\rm sw} = 300$ kHz; $R_i = 1.4$ mΩ, and time constant of high-pass filter $\tau = 2T_{\rm sw}$. The proposed model agrees with simulation results very well up to $2/3\,f_{\rm sw}$.

Fig. 22 shows the verification for constant frequency V^2 peak control, for OSCON capacitors, $D = 0.4$, $f_{\rm sw} = 300$ kHz, and $S_e = 0.7\ S_f$. For ceramic capacitors, $D = 0.4$, $f_{\rm sw} = 300$ kHz, $R_i = 3.3$ mΩ, and $S_e = 0.7\ S_f$. For both cases, control-to-output voltage transfer function can be designed as a constant

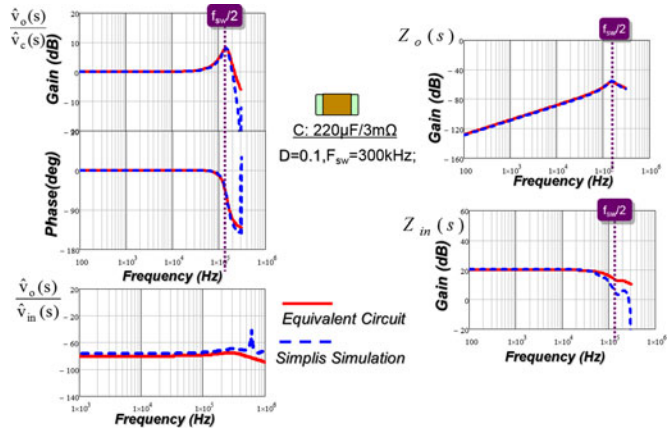

Fig. 20. Simplis verification for constant on-time V^2 control with ceramic capacitors (3 mΩ/220 μF).

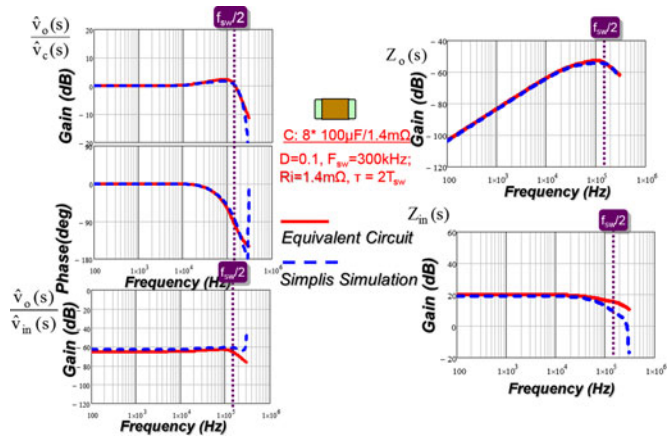

Fig. 21. Simulation verification of equivalent circuit model with inductor current ramp and high-pass filter.

gain up to very high frequency and the model agrees well with simulation result up to $2/3 f_{\rm sw}$.

Fig. 23 shows the experimental waveform based on LM34919 demo-board with the following parameters: $F_{\rm sw} = 900$ kHz; $V_{\rm in} = 15$ V; $D = 0.22$; $V_o = 3.3$ V; $L_s = 10$ μH; and $R_o = 10$ Ω. According to the prediction from the equivalent circuit model, for traditional ceramic capacitors (10 μF/5 mΩ), damping of the double pole caused by the capacitor voltage loop is negative, instability is observed, as shown in Fig. 23(a). With controlled ESR ceramic capacitors CERD1JX5R0J106M (10 μF/50 mΩ), the double pole is well damped and the circuit is stable in Fig. 23(b). From Fig. 24(a), the prediction of control to output voltage transfer function from the equivalent circuit model can match with experimental data up to $2/3 f_{\rm sw}$. Fig. 24(b) shows the verification of audio susceptibility transfer function. Audio susceptibility performance for constant on-time V^2 control is very good as the gain is very low (around -60 dB) in the whole frequency region up to $\frac{1}{2} f_{\rm sw}$. Compared with measurement data, the prediction from the equivalent circuit model is good.

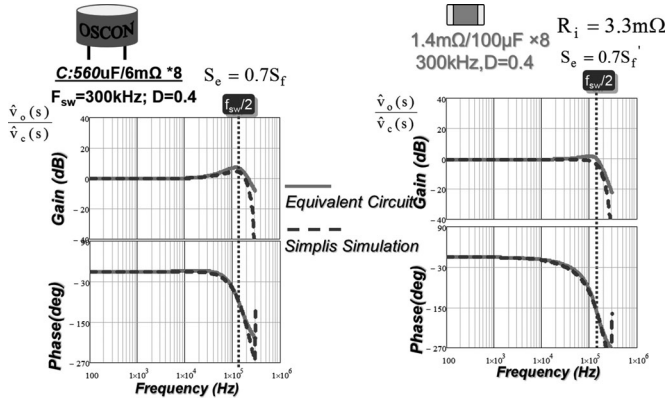

Fig. 22. Simplis verification for constant frequency V^2 peak control. (a) OSCON (6 mΩ/560 μF) with $S_e = 0.7\ S_f$. (b) Ceramic (1.4 mΩ/100 μF) with $R_i = 3.3$ mΩ and $S_e = 0.7\ S_f$.

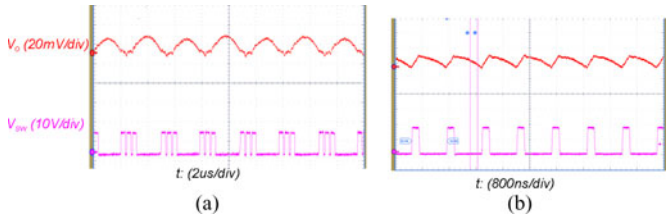

Fig. 23. Experimental waveforms for constant on-time V^2 control. (a) Traditional ceramic capacitors (10 μF/5 mΩ). (b) Controlled ESR ceramic capacitors (10 μF/50 mΩ).

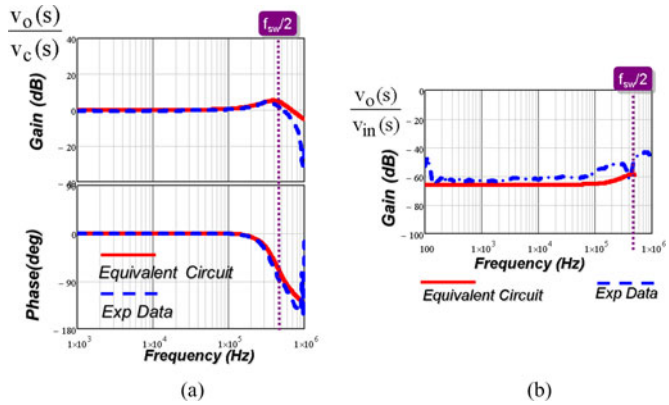

Fig. 24. Experimental verification of transfer functions with controlled ESR ceramic capacitors CERD1JX5R0J106M (10 μF/50 mΩ). (a) Control to output voltage. (b) Audio susceptibility.

To verify the proposed optimal design guideline, Fig. 25 shows the load transient experimental waveforms for constant on-time enhanced V^2 control with high-pass filter, based on TPS51513 evaluation board with the following parameters: $F_{\rm sw} = 300$ kHz; $V_{\rm in} = 12$ V; $V_o = 1.1$ V; $D = 0.1$; $L_s = 0.47$ μH; six ceramic caps (100 μF/2 m Ω); load transient: 3 to 8 A with 2-kHz frequency and 50% duty cycle. In Fig. 25(a), current sensing gain R_i is insufficient and Q_3' shown in (10) is 4, the dynamic performance is very bad. In Fig. 25(b), current sensing gain R_i is optimized to control Q_3' around 1 and transient performance is good. In Fig. 25(c), R_i is too large, the

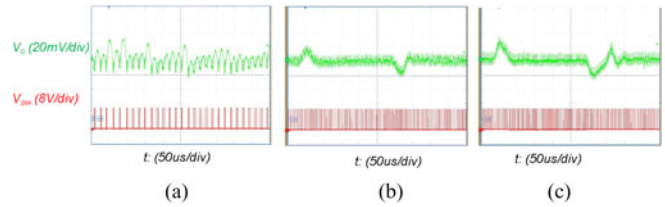

Fig. 25. Comparison of load transient experimental waveforms: (a) with insufficient R_i ($R_i = 0.4$ m, $Q_3' = 4$), (b) with optimized R_i ($R_i = 2$ m, $Q_3' = 1$), and (c) with too large R_i ($R_i = 10$ m, $Q_3' = 0.2$).

settling time, the overshoot and undershoot voltage all increase. The proposed optimal design to control quality factor around 1 provides best transient performance among the three.

VII. Summary and Conclusion

This paper proposed a unified equivalent circuit model of V^2 control. The model represents capacitor voltage sideband effects with a $R_{e2} - L_{e2}$ branch, which forms the double pole by resonating with output capacitor. The equivalent circuit model is a complete model and all the transfer functions are accurate up to switching frequency. The equivalent circuit model has rich physical insight of V^2 control as a nonideal voltage source and is very helpful for design. Design guidelines on controlled ESR ceramic capacitors, current sensing gain R_i, and high-pass filter are presented to provide the good dynamic performance. The unified equivalent circuit model is valid for V^2 control with different modulation schemes and small-signal behaviors between constant frequency V^2 peak control and constant on-time V^2 control are compared, revealing the advantage of constant on-time modulation from stability point of view.

References

[1] D. Goder and W. R. Pelletier, "V^2 architecture provides ultra-fast transient response in switch mode power supplies," in *Proc. High Frequency Power Convers. Conf.*, 1996, pp. 19–23.

[2] D. Goder, "Switching regulators," U.S. Patent 5 770 940, 1998.

[3] (2009, Jul.). Texas Instruments. TPS51116 datasheet. [Online]. Available: http://focus.ti.com/lit/ds/symlink/ tps51116.pdf

[4] (2012, Jun.). Monolithic Power Systems. MP38900 datasheet. [Online]. Available: http://www.monolithicpower.com/

[5] (2007, Oct.). STMicroelectronics. PM6685 datasheet. [Online]. Available: http://www.st.com/.

[6] (2009, Sep.). Maxim. MAX1545 datasheet. [Online]. Available: http://datasheets.maxim-ic.com/en/ds/MAX1519-MAX1545.pdf

[7] (2013, Feb.). National Semiconductor. LM34919 datasheet. [Online]. Available: http://www.national.com/ds/LM/ LM34919.pdf

[8] (2008, Mar.). Intersil. ISL6237 datasheet. [Online]. Available: www.intersil.com/data/fn/fn6418.pdf

[9] (2013, Jan.). Texas Instruments. TPS51220 datasheet. [Online]. Available: http://www.ti.com/lit/ds/symlink/tps51220a.pdf

[10] (2007, Oct.). On-Semi Conductors. NCP5422A datasheet. [Online]. Available: http://www.onsemi.com/

[11] (2012, Oct.). Muruta. MPDRX002S datasheet. [Online]. Available: http://search.murata.co.jp/Ceramy/image/img/A14X/RX002SEA.pdf

[12] J. Sun, "Characterization and performance comparison of ripple based control for voltage regulator modules," *IEEE Trans. Power Electron.*, vol. 21, no. 2, pp. 346–353, Mar. 2006.

[13] R. Redl and J. Sun, "Ripple-based control of switching regulators —An overview," *IEEE Trans. Power Electron.*, vol. 24, no. 12, pp. 2669–2680, Dec. 2009.

[14] M. Wang, "Power supply design with fast transient response using V^2 control scheme," in *Proc. Int. IC Conf.*, 1999, pp. 189 –199.

[15] W. Huang and J. Clarkin, "Analysis and design of multiphase synchronous buck converter with enhanced V^2 control," in *Proc. High Frequency Power Convers. Conf.*, 2000, pp. 74–81.

[16] W. Huang, "A new control for multi-phase buck converter with fast transient response," in *Proc. IEEE Appl. Power Electron. Conf.*, Anaheim, CA, USA, 2001, pp. 273–279.

[17] K. Lee, K. Yao, X. Zhang, Y. Qiu, and F. C. Lee, "A novel control method for multiphase voltage regulators," in *Proc. IEEE Appl. Power Electron. Conf.*, 2003, pp. 738–743.

[18] T. Noma, "Muruta's high-speed DC/DC converter tames fast load transient," in *AEI Dempa Publications, Inc.*, pp. 31–34, Apr. 2006.

[19] Y. Mai and P. Mok, "A constant frequency output-ripple-voltage-based buck converter without using large ESR capacitor," *IEEE Trans. Circuits Syst. II, Exp. Briefs*, vol. 55, no. 8, pp. 748–752, Aug. 2008.

[20] Y. Lee, S. Wang, and K. Chen, "Quadratic differential and integration technique in V^2 control buck converter with small ESR capacitor," *IEEE Trans. Power Electron.*, vol. 25, no. 4, pp. 829–838, Apr. 2010.

[21] M. Viejo, P. Alou, J. Oliver, O. Garcia, and J. Cobos, "V^{2}Ic control: A novel control technique with very fast response under load and voltage steps," in *Proc. IEEE Appl. Power Electron. Conf.*, 2011, pp. 231–237.

[22] J. Cortes, V. Svikovic, P. Alou, J. Oliver, and J. Cobos, "Comparison of the behavior of voltage mode, V^2 and V^{2}Ic control of a buck converter for a very fast and robust dynamic response," in *Proc. IEEE Appl. Power Electron. Conf.*, 2014, pp. 2888–2894.

[23] G. Zhou, J. Xu, and J. Wang, "Constant-Frequency peak-ripple-based control of buck converter in CCM: Review, unification, and duality," *IEEE Trans. Ind. Electron.*, vol. 61, no. 3, pp. 1280–1291, Mar. 2014.

[24] G. Zhou, J. Xu, J. Sha, and Y. Jin, "Valley V^2 control technique for switching converters with fast transient response," in *Proc. IEEE Int. Conf. Power Electron., Energy Convers. Congr. Expo.*, 2011, pp. 2788–2791.

[25] X. Zhou, J. Fan, and A. Huang, "Monolithic DC offset self-calibration method for adaptive on-time control buck converter," in *Proc. IEEE Energy Convers. Congr. Expo.*, 2009, pp. 655–658.

[26] Y. Lin, C. Chen, D. Chen, and B. Wang, "A ripple-based constant on-time control with virtual inductor current and offset cancellation for DC power converters," *IEEE Trans. Power Electron.*, vol. 27, no. 10, pp. 4301–4310, Oct. 2012.

[27] C. Tsai, S. Lin, and C. Huang, "A fast-Transient quasi-V^2 switching buck regulator using AOT control with a load current correction (LCC) technique," *IEEE Trans. Power Electron.*, vol. 28, no. 8, pp. 3949–3957, Aug. 2013.

[28] W.Chen, C. Wang, Y. Su, Y. Lee, C. Lin, K. Chen, and M. Du, "Reduction of Equivalent series inductor effect in delay-ripple reshaped constant on-time control for buck converter with multilayer ceramic capacitors," *IEEE Trans. Power Electron.*, vol. 28, no. 5, pp. 2366–2376, May 2013.

[29] Y. Yan, P. Liu, F. C. Lee, Q. Li, and S. Tian, "V^2 control with capacitor current ramp compensation using lossless capacitor current sensing," in *Proc. IEEE Energy Convers. Congr. Expo.*, 2013, pp. 117–124.

[30] W. Chen, J. Chen, T. Liang, L. Wei, J. Huang, and W. Ting, "A novel quick response of RBCOT with VIC ripple for buck converter," *IEEE Trans. Power Electron.*, vol. 28, no. 9, pp. 4299–4307, Sep. 2013.

[31] K. Cheng, F. C. Lee, and P. Mattavelli, "Adaptive ripple-based constant on-time control with internal ramp compensations for buck converter," in *Proc. IEEE Appl. Power Electron. Conf.*, 2014, pp. 440–446.

[32] T. Miyazaki and T. Ogawa, "Constant on-time DC-DC converter using ripple injection filter with inherent adaptive voltage positioning," in *Proc. IEEE Appl. Power Electron. Conf.*, 2014, pp. 460–463.

[33] S. Qu, "Modeling and design considerations of V^2 controlled buck regulator," in *Proc. IEEE Appl. Power Electron. Conf.*APEC, Anaheim, CA, USA, 2001, pp. 507–513.

[34] F. Wang, J. F. Xu, and J. P. Xu, "Small-signal model of V^2 control technique with compensation," in *Proc. IEEE Int. Conf. Commun. Circuits Syst.*, 2004, pp. 1358–1362.

[35] S. He, S. Wu, Y. Xu, T. Yan, Y. Chen, and L. Chen, "Nonlinear modeling and analysis of valley V^2 controlled buck converter," in *Proc. IEEE Int. Conf. Microw. Antenna Propag. EMC Technol. Wireless Commun.*, 2013, pp. 659–663.

[36] J. Wang, J. Xu, and B. Bao, "Analysis of pulse bursting phenomenon in constant-on-time-controlled buck converter," *IEEE Trans. Ind. Electron.*, vol. 58, no. 12, pp. 5406–5410, Dec. 2011.

[37] J. Wang, B. Bao, J. Xu, G. Zhou, and W. Hu, "Dynamical effects of equivalent series resistance of output capacitor in constant on-time controlled buck converter," *IEEE Trans. Ind. Electron.*, vol. 60, no. 5, pp. 1759–1768, May 2013.

[38] C. Fang, "Closed-form critical conditions of instabilities for constant on-time controlled buck converters," *IEEE Trans. Circuits Syst.*, vol. 59, no. 12, pp. 3090–3097, Dec. 2012.
[39] C. Fang, "Critical conditions for a class of switched linear systems based on harmonic balance: Application to DC-DC converters," *Nonlinear Dyn.*, vol. 70, no. 3, pp. 1767–1789, Nov. 2012.
[40] C. Fang and R. Redl, "Subharmonic stability limits for the buck converter with ripple-based constant on-time control and feedback Filter," *IEEE Trans. Power Electron*., vol. 29, no. 4, pp. 2135–2142, Apr. 2014.
[41] C. Fang, "Instability conditions for a class of switched linear systems with switching delays based on sampled-data analysis: Application to DC-DC converters," *Nonlinear Dyn.*, vol. 77, nos. 1/2, pp. 185–208, Jul. 2014.
[42] J. Cortes, V. Svikovic, P. Alou, J. Olive, J. Cobos, and R. Wisniewski, "Accurate analysis of subharmonic oscillations of V^2 and V^2Ic controls applied to buck converter," *IEEE Trans. Power Electron*., vol. 30, no. 2, pp. 1005–1018, Feb. 2015.
[43] T. Qian, and W. Wu, "Analysis of the ramp compensation approaches to improve stability for buck converters with constant-on-time control," *IET Power Electron.*, vol. 5, no. 2, pp. 196–204, 2012.
[44] T. Qian, "Study of sub-harmonic oscillation mechanism and effect of circuit propagation delay for buck converters with constant on-time control," *IEEE Trans. Circuits Syst.*, vol. 60, no. 3, pp. 3090–3097, Mar. 2013.
[45] T. Qian, "Subharmonic analysis for buck converters with constant on-time control and ramp compensation," *IEEE Trans. Ind. Electron*. vol. 60, no. 5, pp. 1780–1786, May 2013.
[46] J. Li and F. C. Lee, "Modeling of V^2 current-mode control," *IEEE Trans. Circuits Syst. I, Reg. Papers*, vol. 57, no. 9, pp. 2552–2563, Sep. 2009.
[47] F. Yu and F. C. Lee, "Design oriented model for constant on-time V^2 control," in *Proc. IEEE Energy Convers. Congr. Expo.*, 2010, pp. 3115–3122.
[48] Y. Yan, F. C. Lee, P. Mattavelli, and S. Tian," Small signal analysis of V^2 control using current mode equivalent circuit Model," in *Proc. IEEE Appl. Power Electron. Conf.*, 2013, pp. 1709–1716.
[49] F. Yu, F. C. Lee, and P. Mattavelli, "A small signal model for V^2 control with composite output capacitors based on describing function approach," in *Proc. IEEE Energy Convers. Congr. Expo.*, 2011, pp. 1236–1243.
[50] S. Tian, F. C. Lee, Q. Li, and Y. Yan, "Unified equivalent circuit model of V^2 control," in *Proc. IEEE Appl. Power Electron. Conf.*, 2014, pp. 1016–1023.
[51] S. Tian, F. C. Lee, P. Mattavelli, and Y. Yan, "Small-signal analysis and optimal design of constant frequency V^2 Control," *IEEE Trans. Power Electron*., vol. 30, no. 3, pp. 1724–1733, Mar. 2015.
[52] (2012, Jan.). Texas Instruments. 3-phase+1-phase, D-CAP+ step down controller for IMVP7 CPU/GPU Vcore, TPS59650 datasheet. [Online]. Available: http://www.ti.com/lit/ds/symlink/tps59650.pdf
[53] (2009, Jul.). 3-phase+1-phase, quick-PWM controller for VR12/IMVP7. MAX17039 datasheet. [Online]. Available: http://www.maximintegrated.com/en/products/power/MAX17039.html
[54] M. Togashi, "ESR control multilayer ceramic caps," TDK tech. rep., High-Technology, 2008 Ed., Jun. 2008.
[55] K. Cheng, S. Tian, F. Yu, F. C. Lee, and P. Mattavelli, "Digital hybrid ripple-based constant on-time control for voltage regulator modules," *IEEE Trans. Power Electron.*, vol. 29, no. 6, pp. 3132–3144, Jun. 2014.
[56] S. Tian, F. Lee, P. Mattavelli, K. Cheng, and Y. Yan, "Small-signal analysis and optimal design of external ramp for constant on-time V^2 control with multilayer ceramic caps," *IEEE Trans. Power Electron*., vol. 29, no. 8, pp. 4450–4460, Aug. 2014.
[57] V. Vorperian, "Simplified analysis of PWM converters using model of PWM switch. Continouous conduction mode," *IEEE Trans. Aerosp. Electron. Syst*., vol. 26, no. 3, pp. 490–496, May 1990.
[58] Y. Yan, F. C. Lee, and P. Mattavelli, "Unified three-terminal switch model for current mode controls," *IEEE Trans. Power Electron*., vol. 27, no. 9, pp. 4060–4070, Sep. 2012.
[59] S. Tian, F. C. Lee, J. Li, Q. Li, and P. Liu, "Equivalent circuit model of constant on-time current mode control with external ramp compensation," in *Proc. IEEE Energy Convers. Congr. Expo.*, 2014, pp. 3747–3754.
[60] R. B. Ridley, "A new, continuous-time model for current-mode control," *IEEE Trans. Power Electron*., vol. 6, no. 2, pp. 271–280, Apr. 1991.
[61] J. Li and F. C. Lee, "New modeling approach and equivalent circuit representation for current mode control," *IEEE Trans. Power Electron*., vol. 25, no. 5, pp. 1218–1230, May 2010.
[62] Y. Qiu, M. Xu, K. Yao, J. Sun, and F. C. Lee, "Multi-frequency small-signal model for Buck and multi-phase Buck converters," *IEEE Trans. Power Electron*., vol. 21, no. 5, pp. 1185–1192, Sep. 2006.
[63] G. W. Wester and R. D. Middlebrook, "Low frequency characterization of switched dc-to-dc converters," in *Proc. IEEE Power Process. Electron. Spec. Conf.*, 1972, pp. 9–20.
[64] P. Liu, Y. Yan, F. C. Lee, and Q. Li, "Auto-tuning and self-calibration techniques for V^2 control with capacitor current ramp compensation using lossless capacitor current sensing," in *Proc. IEEE Energy Convers. Congr. Expo.*, 2014, pp. 117–124.

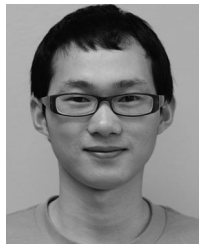

Shuilin Tian (S'11) received the B.S. degree in electrical engineering from Zhejiang University, Hangzhou, China, in 2008, and the M.S. degree in power electronics from the Center for Power Electronics Systems, Virginia Tech, Blacksburg, VA, USA, in April 2012, where he is currently working toward the Ph.D. degree.

From May 2012 to August 2012, he was an Application Engineer Intern in Linear Technology, Milpitas, CA, USA. His research interests include modeling, analysis, control of PWM converters (including point of load converters and voltage regulator), and resonant converters.

Fred C. Lee (S'72–M'74–SM'87–F'90) received the B.S. degree in electrical engineering from National Cheng Kung University, Tainan City, Taiwan, in 1968, and the M.S. and Ph.D. degrees in electrical engineering from Duke University, Durham, NC, USA, in 1972 and 1974, respectively.

He is currently a University Distinguished Professor at Virginia Polytechnic Institute and State University (Virginia Tech), Blacksburg, VA, USA, and the Founder and Director of the Center for Power Electronics Systems. He holds 72 U.S. patents, and has published 252 journal articles and 639 refereed technical papers.

Dr. Lee has served as the President of the IEEE Power Electronics Society during 1993–1994 and received the William E. Newell Power Electronics Award in 1989, the Arthur E. Fury Award for Leadership and Innovation in 1998, the Honorary Sun Yuen Chuan Chair Professor at National Tsinghua University, Taiwan, in 2001, the Outstanding Alumni Award from National Cheng Kung University in 2004, the Ernst-Blickle Award for achievement in the field of power electronics in 2005, and the Honorary Kwoh-Ting Li Chair Professor Award at National Cheng Kung University in 2011. He is a Member of the National Academy of Engineering in United States and an academician of Academia in Taiwan.

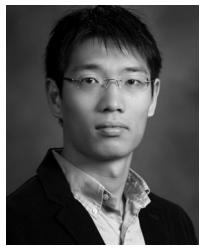

Qiang Li (M'12) received the B.S. and M.S. degrees in power electronics from Zhejiang University, Hangzhou, China, in 2003 and 2006, respectively, and the Ph.D. degree from Virginia Tech, Blacksburg, VA, USA, in 2011.

He is currently an Assistant Professor at the Center for Power Electronics Systems at Virginia Tech. His research interests include distributed power systems, high-frequency power conversion, and high-density electronics packaging and integration.

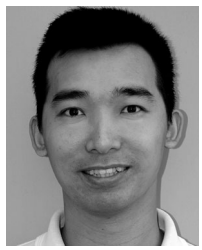

Yingyi Yan (S'10–M'13) received the Bachelor degree from Zhejiang University, China, in 2007. He received the M.S. and Ph.D. degrees in 2010 and 2013 respectively, both in power electronics from Center for Power Electronics Systems at Virginia Tech. He has been with Linear Technology since 2013. He was an application engineer for the high current power solutions and digital Power System Management products. He is now an IC designer for power management products. His research interests include modeling and analysis of power converters, advanced control techniques and high-frequency power conversion.